energies

MDPI

Article

Conversion and Testing of a Solar Thermal Parabolic Trough Collector for CPV-T Application

Richard Felsberger *, Armin Buchroithner, Bernhard Gerl and Hannes Wegleiter

Institute of Electrical Measurement and Sensor Systems, Graz University of Technology, 8010 Graz, Austria; armin.buchroithner@tugraz.at (A.B.); bgerl@tugraz.at (B.G.); wegleiter@tugraz.at (H.W.)

* Correspondence: richard.felsberger@tugraz.at; Tel.: +43-316-873-30526

Received: 20 October 2020; Accepted: 12 November 2020; Published: 23 November 2020

Abstract: In the field of solar power generation, concentrator systems, such as concentrator photovoltaics (CPV) or concentrated solar power (CSP), are subject of intensive research activity, due to high efficiencies in electrical power generation compared to conventional photovoltaics (PV) and low-cost energy storage on the thermal side. Even though the idea of combining the thermal and electrical part in one absorber is obvious, very few hybrid systems (i.e., concentrator photovoltaics-thermal systems (CPV-T)) are either described in literature or commercially available. This paper features the conversion of a commercial thermal parabolic trough collector to a CPV-T hybrid system using multi-junction PV cells. The design process is described in detail starting with the selection of suitable PV cells, elaborating optical and mechanical system requirements, heat sink design and final assembly. Feasibility is proven by practical tests involving maximum power point tracking as well as empirical determination of heat generation and measurement results are presented.

Keywords: concentrator photovoltaic; parabolic trough; concentrated solar power; multi-junction cell; CSP; CPV; CPV-T

1. Introduction

According to the International Energy Agency (IEA), "Solar PV showed record 40% growth in power generation in 2017 and is well on track to meet its Sustainable Development Scenario (SDS) target, which requires average annual growth of 17% from 2017 to 2030" [1]. The constant growth and market potential in the photovoltaic (PV) sector are undeniable, but according to some studies, such as [2], the global potential of concentrated solar power (CSP) is even considerably larger than the present world electricity consumption.

CSP Technology

CSP refers to any technology using the sun's direct normal irradiance (DNI) and focusing it on an absorber to generate heat for later conversion to electricity via a steam turbine, Stirling engine, or similar. While there may have been numerous early historic attempts to focus sunlight and use generated heat to evaporate water or start fires, the first well documented concentrated solar power plants (nearly all of them parabolic trough) were designed in the late 1960s to early 1980s [3]. Meanwhile, CSP faculties have evolved to elaborate, large industrial power plants offering several hundred MWs of power and incorporating cost-effective thermal energy storage [4]. Solar power towers (also known as central receiver CSP) and parabolic trough collectors hold the largest share within this field, but Fresnel reflectors and dish Stirling systems have also emerged on the scene (an overview can be seen in Figure 1).

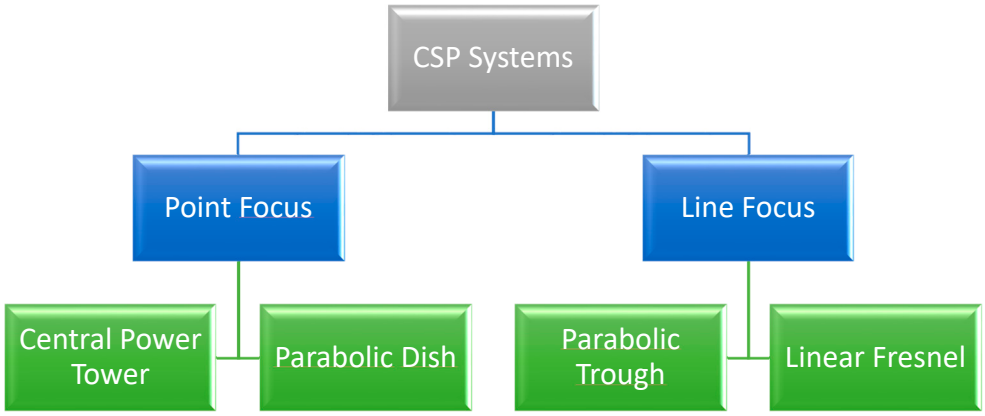

Figure 1. Overview of main concentrating solar power technologies.

CPV Technology

Concentrator photovoltaic (CPV) is an alternative to conventional ("flat-plate") silicon-based PV systems for the cost-effective generation of electricity from solar energy [5]. The main principle behind CPV technology is the drastic reduction of active cell area (raw materials) through the use of cost-effective optical "concentrator elements" (mirrors and lenses). The solar radiation can be amplified up to a factor of 1500, making the more expensive but much more efficient multi-junction cells highly profitable [6]. In this case, one speaks of high concentrator photovoltaics (HCPV).

CPV modules achieve efficiencies far beyond those possible with classic flat-plate PV collectors and, from today's perspective, have a much greater potential for further efficiency increases [7]. CPV cells currently available on the market, e.g., from the company Azurspace, achieve efficiencies of up to 42.1% [6]. The highest efficiency to date was achieved by NREAL at 47.1% [8], with an even further increase to 50% predicted in the coming years [5]. On a global scale, CPV systems with approximately 370 MWp are currently installed and connected to the grid [7].

Structure of Concentrator Photovoltaic (CPV)

Typically, two optical components are used: "Primary Optics" (PO), whose task it is to focus the direct solar irradiance (DNI) and "Secondary Optics" (SO), which is used to distribute the radiation homogeneously on the CPV cell. An overview can be seen in Figure 2.

In the past, parabolic dish concentrators or Fresnel lenses have been most commonly used. In order to focus the sunlight exactly on the CPV cell and to keep it in focus, actuators for sun tracking are required. In recent years, significant improvements have been achieved in the area of sun-tracking mechanisms, especially with respect to cost reduction and reliability. This aspect is important because the tracker mechanism accounts for about one-third of the total cost of a CPV system. [7]

In any case of the above-mentioned technologies, overall system efficiencies, especially when electrical energy is desired are still fairly low, resulting in a rather large demand for real estate/land when CSP projects are realized. Furthermore, falling prices in the flat plate PV sector, primarily driven by China, have threatened the profitability of CSP technology in recent years [7,9]. From a scientific point of view, however, there are significant advantages of CSP (e.g., extremely economic thermal energy storage) and still untapped potential, such as the combination with concentrator photovoltaic (CPV) cells as discussed in the subsequent section.

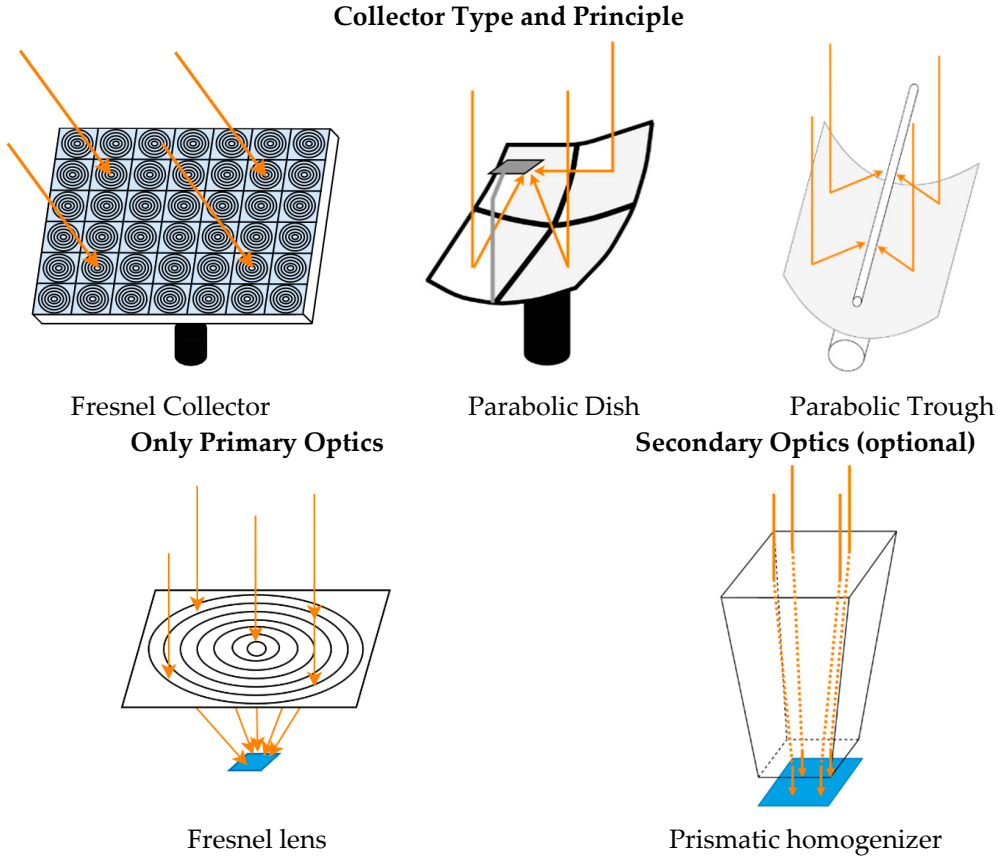

Figure 2. Concepts of concentrator photovoltaics (CPV) systems.

1.1. Motivation

As stated in the introduction, both technologies, CSP and CPV, may play an increasingly important role in the energy revolution, mainly due to the reasons explained below. In contrast to regular silicone PV cells, which seem to have plateaued in terms of efficiency, concentrator PV cells (especially multi junction cells) are gaining ever higher efficiencies, with 50% being within reach [5]. However, three significant disadvantages of CPV technology must be mentioned:

1. The required raw materials are relatively expensive, and hence uneconomic when large surface areas are needed.
2. Since CPV cells are usually operated under high concentration of sunlight, a heat rejection system (i.e., active cooling) is needed.
3. CPV and CSP systems require sun-tracking mechanisms as they can only exploit direct and not global irradiance.

These disadvantages can be avoided by applying CPV cells on an existing CSP system, in the way that

(a) The existing mirror of the collector is used to focus the light on the cell.
(b) The existing absorber tube is used as an active back side cooling system for the cell.
(c) The tracking mechanism is used for the CPV-cell and the thermal collector at once.

By applying these ideas in a smart design, CPV-T can be highly competitive and offers an alternative energy source to many industrial processes that have been powered with fossil fuels in the past.

Versatile Applications of Modern CPV-T Systems

In general, CPV-T technologies are relevant to all regions with high DNI, since electricity and process heat is needed in nearly all industrial applications as well as for domestic building and district energy supply. Based on the "IEA SHC Task 33 and SolarPACES Task IV: Solar Heat for Industrial Processes" [10], CPV-T systems can serve a great variety of applications, the most promising of which are

- Desalination and fresh water generation [11,12].
- Solar cooling [13,14].
- Building heating/cooling and electricity supply [15–17].

Since CPV-T systems are capable of supplying both, electric and thermal energy for the above-mentioned applications, they are ideal for energy self-sufficient solutions. At first glance, the limited temperature level of a CPV-cell (see Sections 2.1 and 2.4 for more details) seems like a major constraint, since it must be kept below 110 °C but the study "ECOHEATCOOL" [18] reports that

- 65% of machinery,
- 61% of transport equipment,
- 58% of mining and quarrying,
- 58% of food and tobacco,
- 50% of other industries,

require heat at temperatures below 100 °C.

Figure 3 shows the schematics of a possible integration of a CPV-T collector in a solar cooling facility.

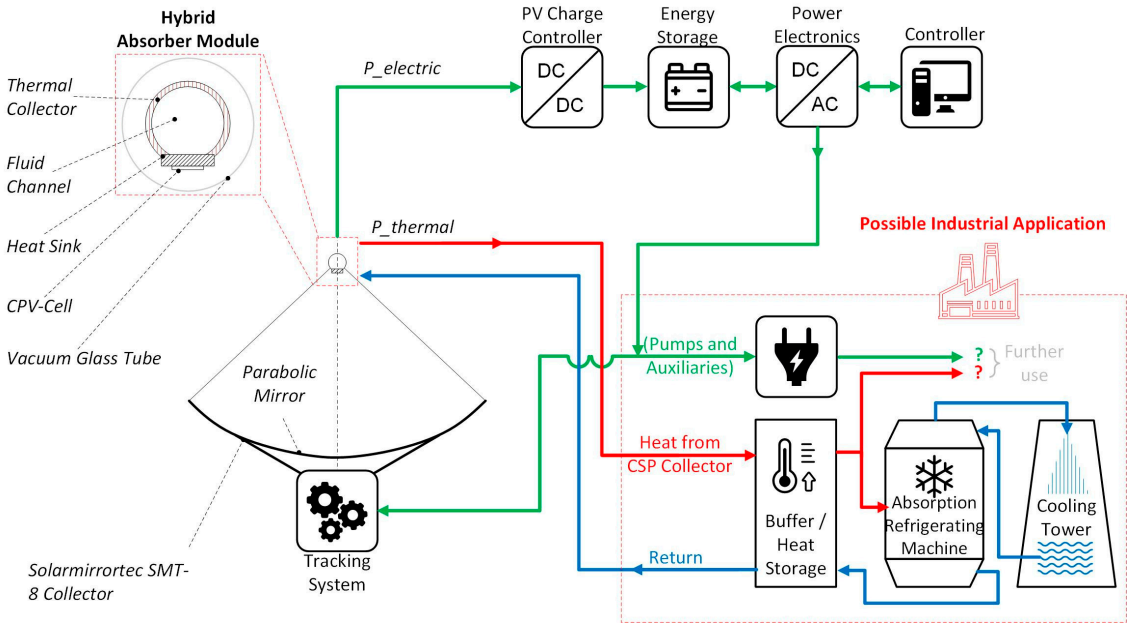

Figure 3. Schematics of solar cooling as a possible industrial application of a CPV-T system involving a parabolic trough collector and CPV-cells.

1.2. State of the Art in CPV-T Systems

The history of CPV-T started in the late 1970s as a further development of flat plate PV-T systems by adding optical concentrator element (e.g., conical concentrator, parabolic trough, spot Fresnel lenses, or linear Fresnel reflectors) to decrease the required PV surface area by maintaining high power output [19].

One of the earliest tests regarding CPV-T systems were conducted by Gibart [20] and Buffet [21], who built one of the first parabolic trough systems that could work with concentration factors of 10× to 40×. Their results showed lower electrical efficiencies than conventional flat PV panels, but higher efficiencies than flat plate thermal collectors.

Rios et al. [22] were one of the first who build a parabolic trough system, which was very cost effective and demonstrated that CPV-T technology was already cheaper than conventional natural gas technologies for electrical and thermal energy demands.

Important research on CPV-T systems with parabolic troughs combined with silicon cells has been done by Coventry [23]. He performed tests on silicon cells and stated that at a concentration of 30× suns, most silicon cells can reach efficiencies of 20% when the temperature of the cell is held at 25 °C. In this test he varied the concentration factor to investigate how different spatial distributions over the cell surface would decrease the cell efficiency. His experiments revealed that a 30× concentration across the entire cell surface results in a 20.6% efficiency, compared to that an increased concentration factor of 90× suns over one-third of the cell the efficiency decreases to 19.4% at 25 °C.

Col et al., have been working on parabolic trough cogeneration systems since roughly 2012. One collector unit, with a size of 3.45 m^2 is supposed to hold 22 multi junction 10 × 10 mm^2 cells (34% electrical efficiency) and produce up 0.5 kW electric and 1.25 kW thermal power [24]. The system is now marketed by Greenetica Srl; however, there is no price information on this relatively complex system [25].

Additional attempts to increase the share of electrical energy output of a CPV-T system are developed by Riahia et al. [26]. They combined mono-crystalline silicon cells with thermoelectric generators. A so called concentrated photovoltaic thermal thermoelectric (CPV-T-TE) system was developed, in which the total extracted electrical energy was increased by 7.46% compared to the CPV-T solar system. The economic feasibility of such systems using expensive Peltier elements is yet to be proven.

Fan Yang et al. [27] pursued a different approach to reduce to overall cost by using a quasi-parabolic concentrator with a low concentration factor and the application of significantly less cost-intensive silicon photovoltaic cells instead of multi-junction CPV cells. The cooling channel for the Si-cells is attached to the rear side of the cells to gain the advantage of the higher overall efficiencies of the CPV-T system.

Table 1 gives an overview of the most important characteristics and specifications of the above-mentioned systems.

Table 1. Overview of important research and development activities in the CPV-T sector.

Authors	Year	Concentrator	Absorber Technology	Cell Type	Efficiency in %
Gibart [20]	1981	Parabolic trough	CPV-T	-	-
Rios et al. [22]	1981	Parabolic trough	CPV-T	-	-
Coventry [23]	2003	Parabolic trough	CPV-T	Si	68%
Col et al. [24]	2014	Parabolic trough	CPV-T	Multijunction	55–70%
Yang et al. [27]	2018	Quasi parabolic mirror	CPV-T	Si	57%
Riahia et al. [26]	2020	Parabolic trough	CPV-T-TE	Si	53%

Since the scope of this work is to describe the design and testing process of a prototype, and not the elaborate discussion of other systems, detailed studies of past and current research in CPV-T can be found in [19,28], respectively.

1.3. Idea and Initial Situation

The idea of this project was to retrofit a commercially available, industrial parabolic trough collector, originally designed for solar thermal heat generation for district heating with a CPV-cell array. The basis for this retrofit-project is the model SMT-8 parabolic trough collector from the company IMK

Solarmirrortec located in Seitenstetten in Austria, which relevant specifications are shown in Table 2. A picture of the collector is shown in Figure 4.

Table 2. Specifications of the SMT-8 Parabolic trough collector by IMK Solarmirrotec.

Specification	Value	Unit
Length of facility	26	m
Aperture of mirror	2.2	m
Focal distance	0.8	m
Temperature range	60–120	°C
Heat transfer fluid	Water/Oil	-
Motor type	AC motor	-
Tracking system	1-Axis (East to West)	-
Gear Ratio (whole system)	97600	-
Accuracy of the system in °	0.5	°

Figure 4. Solar–thermal power plant for district heating using IMK Solarmirrortec SMT-8 parabolic trough modules in Seitenstetten, Austria.

2. Design of the CPV-T Retrofit System

This chapter describes the design and conversion process of the SMT-8 parabolic trough collector, from a purely thermal collector to a CPV-T system. A multitude of aspects and interdependencies needed to be considered: from optical properties such as mirror reflectivity, tracking accuracy, and light special uniformity, to solar cell selection and thermal management to cool the cells properly. Figure 5 shows a basic layout of the CPV board and the attachment on the parabolic trough collector. In the following sections, each of the relevant design aspects and component selection will discussed in detail.

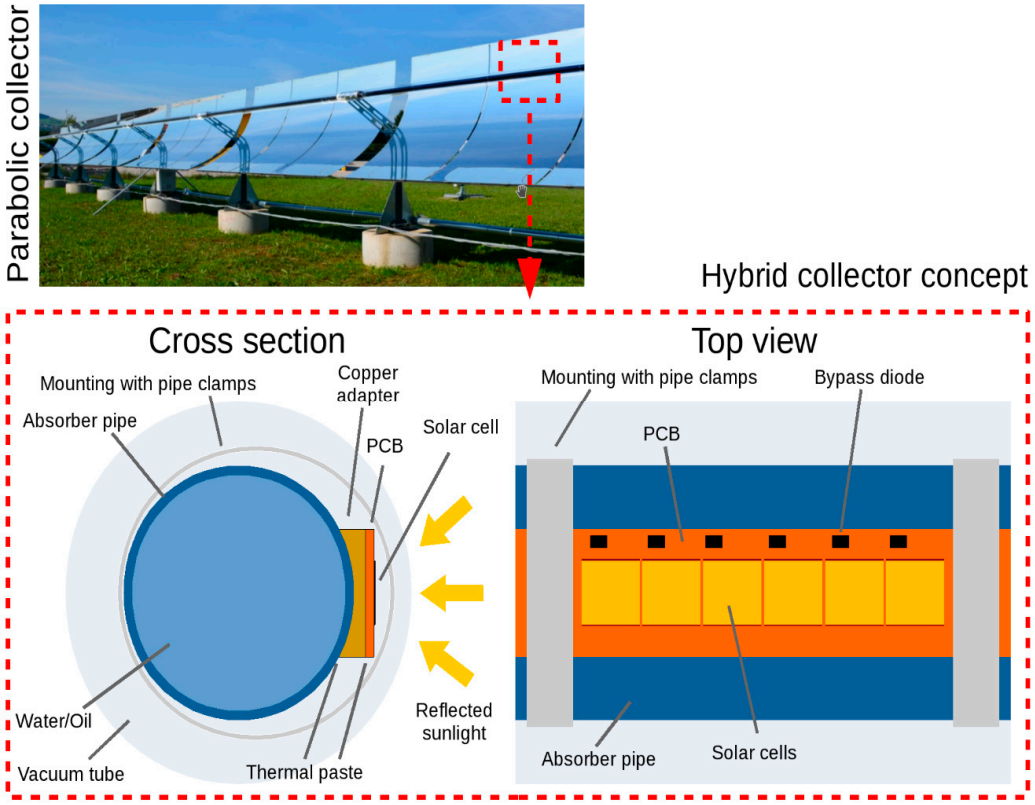

Figure 5. Schematics and principle of the thermo-electric hybrid absorber retrofit concept. The focus point is moved from the center of the tube to the center of the solar cell. This causes most of the irradiation to fall on the solar cell, which in turn dissipates electrical energy and transfers the remaining thermal energy to the heat transfer fluid (HTF) inside the absorber pipe. Since the construction creates a line focus, the solar cells should be packed as close together as possible to achieve the highest possible electrical efficiency.

2.1. Selection of the CPV Cell

The key component to convert a thermal collector into a CPV-T system is the solar cell. The idea is that most of the light reflected by the mirrors falls on the solar cell, which converts the light into electric energy at highest possible efficiency. The remaining energy, which cannot be converted to electricity appears in the form of waste heat and is transferred to the thermal collector. The thermal collector in turn uses its heat transfer fluid (HTF) to cool the cell.

These considerations result in the following requirements for the solar cell:

- **Concentrated sunlight**: In contrast to conventional flat panel solar cells which are designed for normal sun intensities (1× sun), the sunlight in concentrated systems is increased many times by mirrors (e.g., 150 suns, this depends on the mirror geometries and the system structure). This concentration ratio can save solar cell area.
- **Geometry and electrical connectivity suitable for dense packing**: The possibility to mount cells close together in the line focus is crucial to achieve high electrical system efficiencies. Wide spaces between the cells would reduce electrical yield/efficiency significantly, no matter how high the efficiency of the cells themselves are.
- **High operating temperatures**: The maximum cell temperature limits the HTF temperature in the thermal circuit and thus the maximum thermal temperature of the entire system. In order to be able to use the technology in many different industrial processes, the aim is to use a solar cell with a high working temperature (compare Section 1.1).

- **High efficiency and low temperature coefficient**: All in all, the solar cell should have a good degree of efficiency in order to be able to generate a lot of electrical energy. Furthermore, solar cells lose efficiency with increasing temperature (negative temperature coefficient). In order to use the cells effectively in industrial processes with higher temperatures, the temperature coefficient must be as low as possible.
- **Good commercial availability at low cost**: While cell price may be secondary in academic research projects, it will be important for future commercialization. Moreover, the availability of small quantities plays a crucial role for the prototype construction.

Relevant Aspects of Solar Cell Technology

In order to select a suitable solar cell for the envisioned application, it is particularly important to consider the concentration factor (how many times the sunlight is concentrated). Most of the solar cells on the market are silicon based and designed for single sun intensity (1× sun) [29]. All of these cells would have almost no efficiency under concentrated conditions due to their internal structure. Although there are silicon-based cells for concentrated sunlight, the permissible concentration factor is generally low (<100 suns), and the commercial availability is questionable due to the low dissemination in the market [5]. In contrast, there are several commercially available multi-junction cells, designed specifically for concentrator application. These cells are more efficient but also significantly more expensive than silicon-based cells. To compensate the price difference, manufacturers design these cells for concentrated sunlight (100–1500 suns) [6]. Therefore, these cells are very suitable for CPV-T systems.

External Quantum Efficiency

In multi-junction cells, several photo-active layers are stacked on top of each other, each layer responding to a different frequency band of the sunlight's spectrum. This results in approximately twice the efficiency of silicon-based cells (e.g., 42% versus 22%) [6,30]. Figure 6 shows the spectrum of the sunlight (AM 1.5), the external quantum efficiency (EQE, the spectrum used by the solar cells) of a silicon-based cell and of a multi-junction cell (in this case with three layers (triple-junction cell)) in comparison. The increased efficiency of the multi-junction cell also has a downside: due to the stacking of the cells, the cells must be connected in series (results from the physical structure) [5]. If the incident light does not correspond to the solar spectrum (AM 1.5) and, for example, the spectrum for one layer is not available, this inevitably limits the other working cells. This means that the weakest cell is the bottleneck in a multi-junction cell stack. So, care must be taken to ensure that no parts of the sunlight spectrum are lost before they reach the solar cell (e.g., through limited reflectivity of mirrors or transmissivity of glass tubes/other optical components).

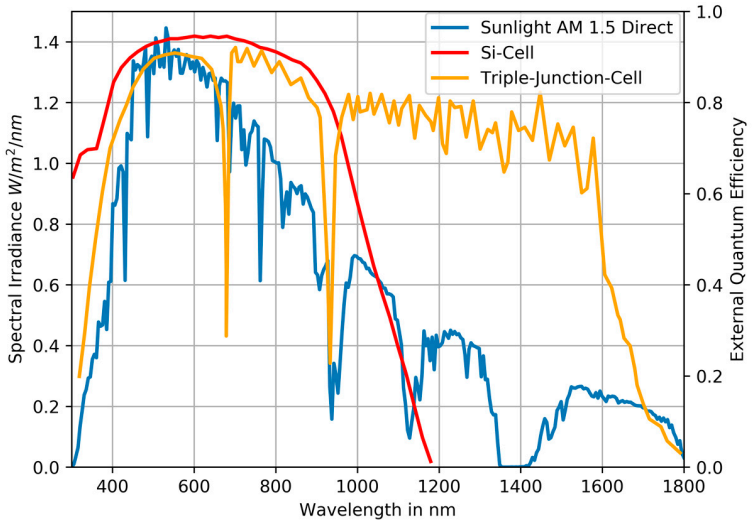

Figure 6. Shows the spectrum of the sunlight (AM 1.5), the external quantum efficiency (EQE) of a silicon-based cell and of a multi-junction solar cell. Data based on [6,30,31].

Sizing and PCB Design

When it comes to size, multi-junction cells typically come in sizes of 3×3 mm^2, 5×5 mm^2 or 10×10 mm^2 [32]. To achieve sufficient electrical output even at high concentration, many of these cells are needed. Each individual cell needs space for its electrical connections. This makes the printed circuit board (PCB) design challenging, especially under the aspect that the cells have to be placed as close as possible to each other in order to get a good system efficiency. In the basic concept in Figure 5, for example, it can be seen how six solar cells are positioned as close together as possible along the line focus. The additional components (bonding connections, bypass diodes, etc.) are positioned outside of the line focus so that no space is wasted in essential areas.

Thermal Management and Cell Efficiency

The maximum permissible operating temperature of the solar cell should be as high as possible in order to allow as many options for industrial heat use as possible (the heat transfer fluid also acts as cooling liquid for the cells). According to some manufacturers, the maximum allowable operating temperature of multi-junction cells is in the range of 110 °C [6]. However, it was shown in [33] that multi-junction cells can be used up to 170 °C. Still, it must be mentioned that under these conditions long-term effects on service life and efficiency are unknown.

However, high operating temperatures are only useful, if the cell's electrical conversion efficiency can be kept high, i.e., a small temperature coefficient is achieved. For multi-junction cells, this coefficient is roughly −0.045%/K, which is about 10 times lower than for silicon-based cells [6,34]. A 100-K-temperature-increase would therefore correspond to an efficiency loss of 4.5%. Particularly in view of the high efficiency of the multi-junction cells of 42% at low operating temperature, this single-digit decrease is still acceptable.

Economic and Commercial Considerations

Finally, the availability and the price of the cell must be considered. The sales market for multi-junction cells is much smaller than the market for silicon-based cells [5]. Nevertheless, there are a few manufacturers where these cells can be bought commercially (e.g., Azurspace, Spectrolab, Emcore, etc.). Additionally, smaller quantities for prototyping are sometimes available there.

The price for higher quantities and the smaller cell area resulting from the concentration factor make this technology competitive with standard flat panel solar cells (see Figure 7). Especially, if the thermal parabolic trough collector is intended anyway, and only the electrical side is added.

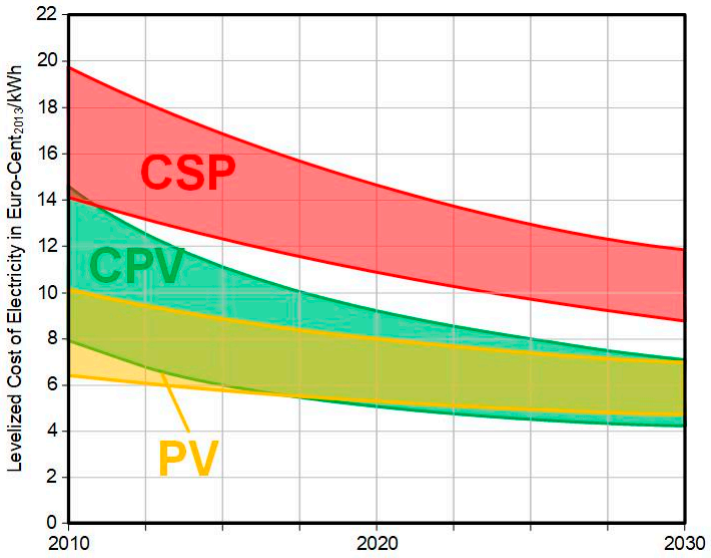

Figure 7. Past development and prognosis of the levelized cost of electricity of PV, concentrated solar power (CSP), and concentrator photovoltaics (CPV) systems in regions of high direct normal irradiance (DNI) (2000 kWh/(m^{2}a)–2500 kWh/(m^{2}a)). Data based on [35].

Considering the previous analysis, it is clear that multi-junction solar cells are well-suited for the CPV-T system. There are some challenges in terms of light spectrum, PCB design, and cooling, but also great opportunities in terms of handling concentrated sunlight, high efficiency, and low temperature coefficients.

2.2. Optical System Requirements

Ideally, the retro-fitted CPV cell is exposed to a homogeneously illuminated area, in which the concentrated sunlight shows so called "pillbox" characteristics. However, even an ideal parabolic mirror cannot provide such radiation distribution, but rather offers a Gaussian distribution. Considering the effect of the absorber tube, which causes partial shading of the mirror, the real distribution can be estimated using FEM simulations (COMSOL with the optical ray tracing module), which are presented in this section.

In Figure 8 the setup of the ray tracing simulation of the parabolic trough is depicted. An artificial sun sends its rays to the parabolic mirror, which redirects them to the focal point of the mirror. The ideal, theoretical focal distance of the simulated mirror (of ideal parabolic shape) is f_d = 800 mm. Several simulations were performed while varying the receiver's distance from the focal point (i.e., distance from the mirror) indicated with "+" and "−" in the subsequent figure to visualize the influence of changes in receiver position (distance of the CPV cell from the theoretical geometric focal point f_d).

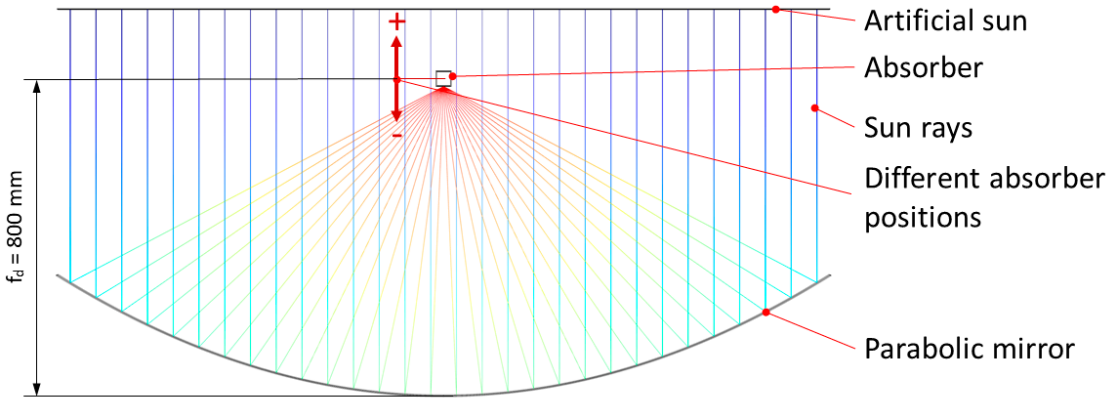

Figure 8. Simulation setup of the FEM ray tracing simulation for receiver placement optimization.

High Concentration Setup

The high concentration setup explores the possibility of mounting one array of 10 mm wide CPV cells perpendicular to each other as shown in Figure 9.

Table 3 gives an overview of the ray tracing simulation results (see Figure 9a). These simulations are marked with $f_d + x$ mm, whereby x indicates the distance from f_d. In position f_d the highest peak flux with the narrowest spatial distribution is reached. The other positions at $f_d + x$ have lower peak fluxes and wider spatial distributions of irradiance. The more the position of the receiver is moved away from its initial position (f_d) the wider the distribution gets and the lower the peak flux becomes.

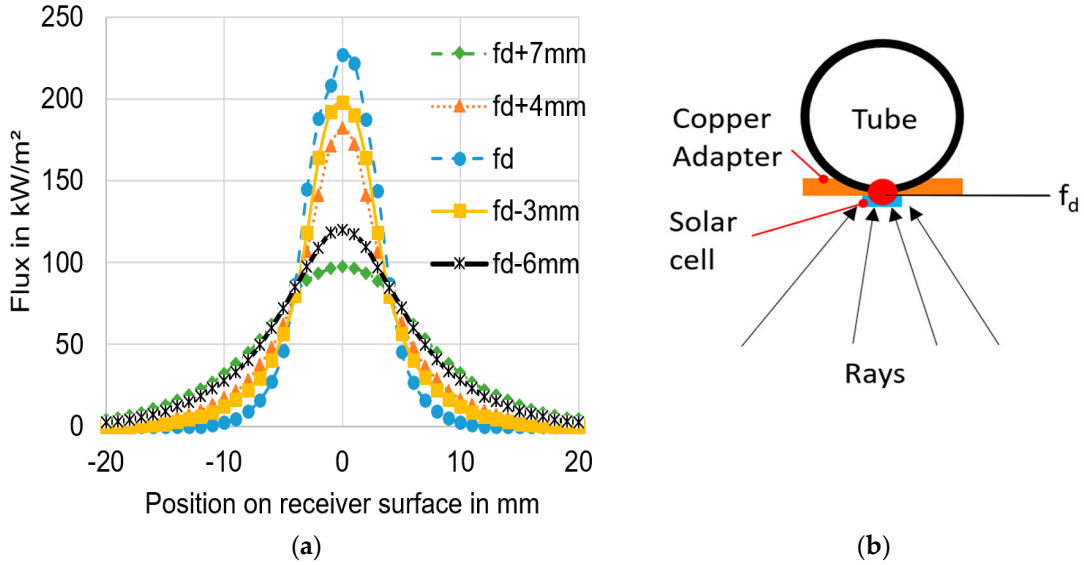

Figure 9. (**a**) Shows the spatial distribution of different receiver positions in the possible high concentration setup. (**b**) Depicts the to (**a**) associated simulation setup, where the focal point f_d is located and how the absorber tube is positioned.

Table 3. Ray tracing simulation of the concentrator parabolic mirror setup to show the influence of the receiver's (CPV cell's) position on peak flux and flux distribution of the high concentration setup.

Position in mm	Spatial Distribution: 40 mm Wide Absorber with 1 CPV Cell	Scale
$f_d + 7$ mm	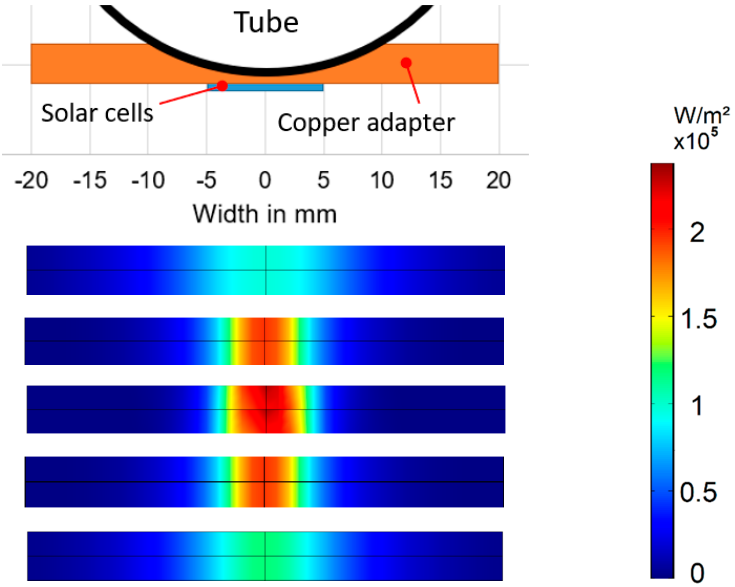	
$f_d + 4$ mm		
f_d		
$f_d - 3$ mm		
$f_d - 6$ mm		

Medium Concentration Setup

The medium concentration setup explores the possibility of mounting two arrays of 10 mm wide CPV cells perpendicular to each other as shown in Figure 10 and Table 4. The advantage would be a higher active cell surface, resulting in higher overall electivity yield but a lower concentration factor and hence twice as many solar cells.

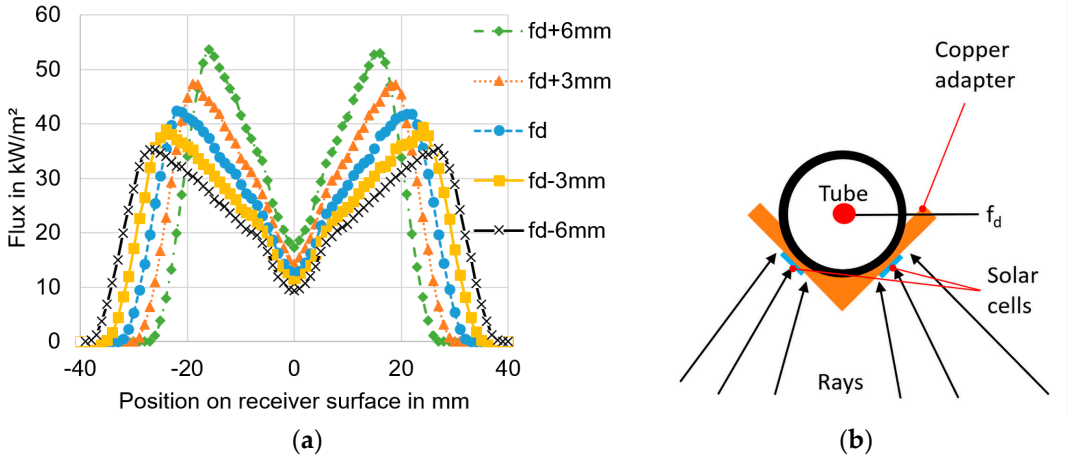

Figure 10. (**a**) Shows the spatial distribution of different receiver positions of the medium concentration setup. (**b**) Depicts the to (**a**) associated simulation setup, where the focal point f_d is located and how the absorber tube is positioned.

Table 4. Ray tracing simulation of the medium concentration setup to depict the influence of the absorber position on peak flux and flux distribution.

Position in mm	Spatial Distribution: 80 mm Wide Absorber with 2 CPV Cells	Scale
f_d + 6 mm	Tube, Solar cells, Copper adapter, Width in mm, -60 -40 -20 0 20 40 60	W/m² x10⁴ 5 4 3 2 1 0
f_d + 3 mm		
f_d		
f_d − 3 mm		
f_d − 6 mm		

Some CPV systems, such as for instance Copper et al. [36] use secondary optics to further concentrate and/or homogenize the light targeted on the cell. However, for reasons of economics and system complexity, a solution avoiding secondary optics was sought. Still, based on the simulations presented above, an absorber position should be chosen allowing the cell to be placed precisely in the focal point f_a = 800 mm.

Mirror reflectivity and glass envelope

A main component of parabolic trough collectors is the mirror. The mirror should have a reflectivity close to 100% over the entire wavelength range of the solar spectrum. Especially with the use of multi-junction cells, which are designed for the solar spectrum air mass 1.5 (AM 1.5), the mirror should have almost no reflection losses in certain wavelength ranges.

To reduce thermal losses at higher temperatures (convection), normally cylindrical glass envelopes are used surrounding the absorber tube to allow evacuation of the surrounding air and hence increased thermal insulation. So, the light has to pass through the glass tube. Therefore, the light spectrum should be as little distorted as possible to ensure efficient operation of the multi-junction cells. At the same time, the glass tube can be used to protect sensitive components of the hybrid absorber from environmental influences.

Angle of incidence of the solar cell

For multi-junction cells, normally high concentration factors should be applied to minimize the cell area. To achieve this, large mirror surfaces are required. This leads to larger light incidence angles at the solar cell (unless the distance between mirror and solar cell increases). Larger angles of incidence cause a loss of efficiency in solar cells. Therefore, a compromise between concentration factor and efficiency reduction must be made.

2.3. Mechanical and Tracking Requirements

As shown in the previous Section 2.2., optical accuracy is essential to achieving reasonable efficiencies. In the case of a concentrator solar collector, mechanical and optical requirements are closely related. For instance:

- Manufacturing tolerances of the support structure affect mirror accuracy (in this case, fidelity of the parabolic shape).
- Structural soundness/stiffness affects optical accuracy during wind loads and gravity sag.
- The gear ratio of tracking system/actuators affects the mechanical "resolution", meaning how precise the sun can be tracked.

These aspects come particularly into play, when (small) CPV cells are used, since a typical thermal absorber tube is much larger and hence does not require such accurate tracking. Sun tracking is usually an intermittent process, meaning that the collector is "bumped" every few seconds to minutes, with the effect that the target is not perfectly centered the entire time, but the focused sunlight rather moves across the cell as the collector is not moving and is then re-centered when tracking occurs.

The effect of this movement across the receiver surface is depicted in Figure 11 and shows that small tracking errors lead to a significant deviation of the flux peak on the receiver surface. Additionally, the peak maximum is decreased with increasing tracking error.

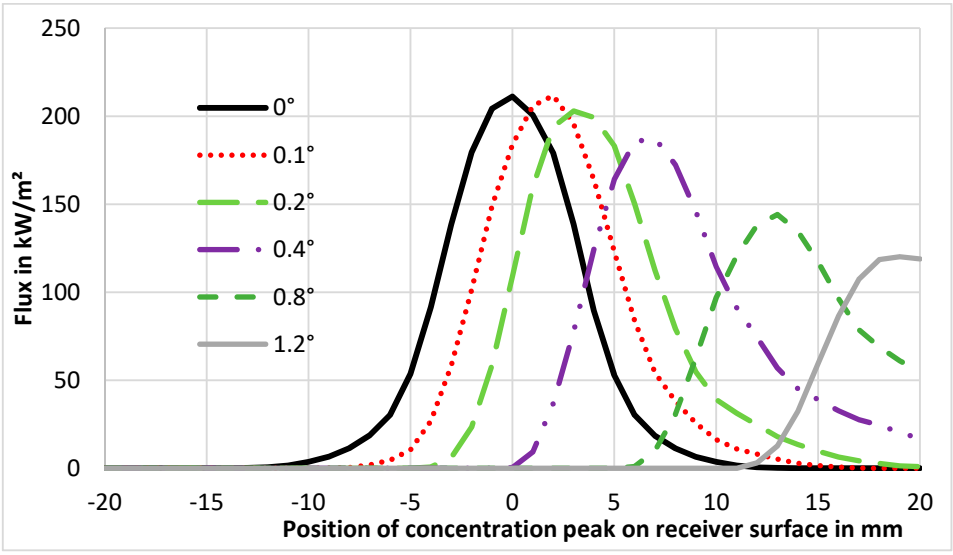

Figure 11. Position of the maximum concentration peak over receiver surface depending on tracking error.

Depending on the following factors, a so called "error budget" can be defined for the CPV-T system:

- Cell size and sensitivity to partial shading.
- Accuracy of tracking system.
- Stiffness of the construction.
- Manufacturing and assembly tolerances.

In the case of the SMT-8 collector prototype equipped with a 10×10 mm^2 CPV cell, this error budget was determined to be around +/−0.116 ° of tracking/mechanical error in order to use 90% of the focused light.

2.4. Heat Rejection and Thermal System

In general, there are two main requirements for the design of the CPV-cell's cooling system/thermal absorber:

- Maintaining cell operating temperature within permissible limits.
- Maximum heat yield and max. temperature level of heat transfer fluid.

In order to achieve these requirements, the thermal resistance between the backside of the CPV cell and the heat transfer fluid must be kept as small as possible. This means that, ideally, the absorber tube is designed with such shape that the cell's board can be mounted directly onto the tube's surface. In the case of the presented prototype, a cylindrical thermal absorber tube with a diameter of 40 mm was used (standard part in CSP systems). A copper adapter (high thermal conductivity) was machined to offer a planar surface for cell mounting and a round contour on the backside for attachment to the tube (see Figure 12).

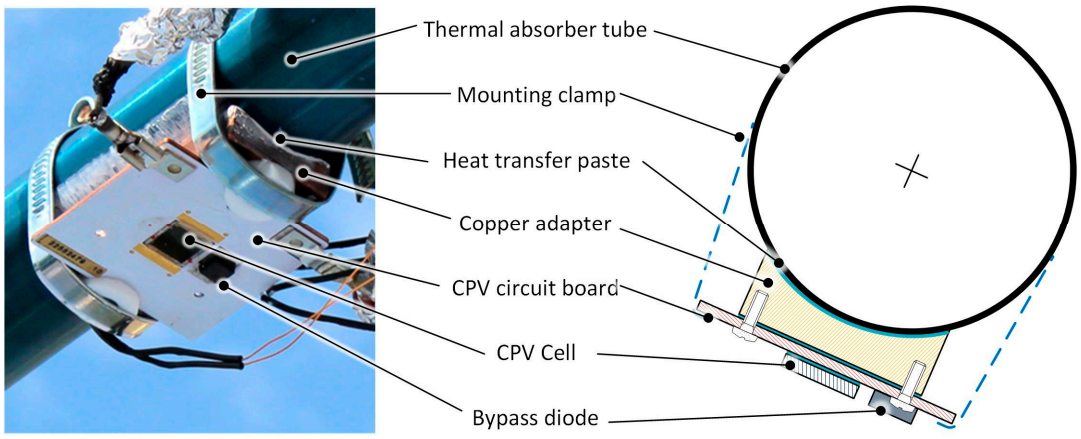

Figure 12. Photo and cross section of the CPV test cell attached to the thermal absorber tube.

Before going into actual field testing the absorber tube was subjected to tests in a solar simulator for several reasons:

(a) To successively increase the concentration factor and ensure the heat rejection system works properly.
(b) To validate FEM simulations of the heat rejection system by applying irradiance in reproducible laboratory conditions.
(c) To validate the functionality of the measurement system (several temperature sensors on the CPV-cell board and in the hydraulic circuit) before field installation.

Figure 13 shows the hybrid absorber setup with a glass envelope in the solar simulator. The test was performed with a concentration ratio of 53 suns (53 kW/m^2) and a heat transfer fluid (HTF) flow

rate of ~12 L/min. The following temperature gradients were obtained, both with and without vacuum: 20 °C HTF temperature leads to 35 °C backside cell temperature and 65 °C HTF leads to 75 °C cell backside temperature. In this configuration, the cell generated 1.09 W (at 25 °C HTF temperature) of electricity, resulting in an efficiency of 20.6%. The low efficiency of the multi-junction cell can be explained by the spectral mismatch of the solar simulator light. The findings from the solar simulator test show that the hybrid absorber design and the measuring system can be used in a test setup with a parabolic trough collector.

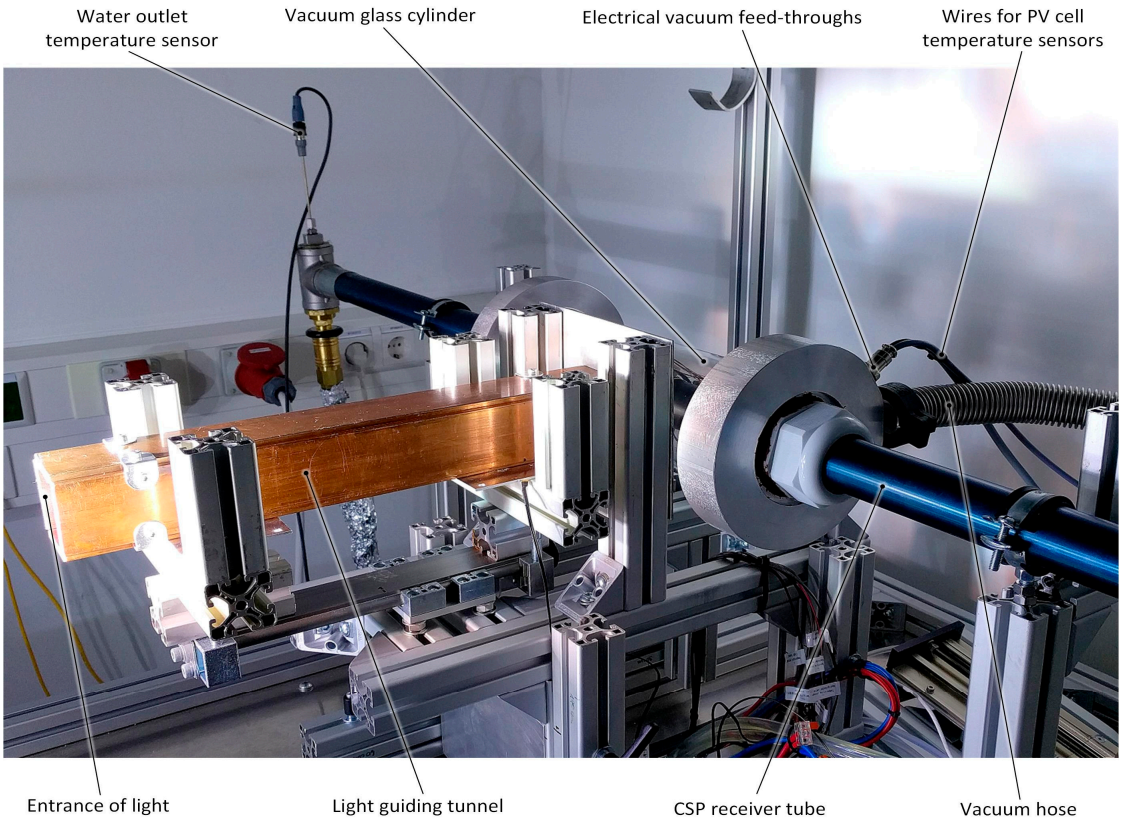

Figure 13. Solar simulator tests with the retrofitted absorber tube.

3. Measurement Results and Discussion

Within the presented project, the previous considerations were put into practice in order to validate the idea of the CPV-T retrofit hybrid system. The test setup is presented first, followed by a presentation and discussion of various results.

3.1. Test Setup

To create a proof of concept of the designed hybrid absorber a 1 m long section of the thermal parabolic trough collector was used for the conversion. In Figure 14 the structure can be seen. It shows the parabolic mirror, the sun tracking system, measurement equipment and the hybrid absorber consisting of a common absorber tube for thermal systems with a CPV solar cell assembly attached to it. Furthermore, it can be seen that the high concentration setup is in use (compare Section 2.2).

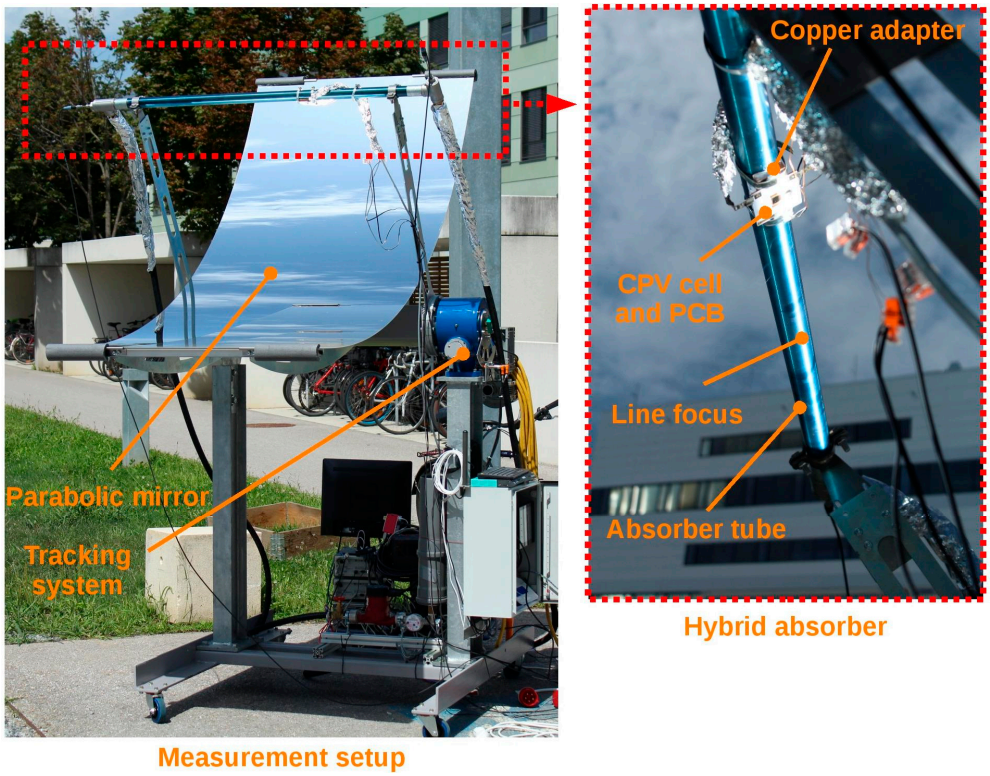

Figure 14. Test setup of the CPV-T hybrid system. Left: Parabolic mirror with the tracking system and the measurement setup. Right: Closer focus on the hybrid absorber with the visible line focus and the multi-junction cell.

In order to test the basic functionality and for reasons of simplicity only a single solar cell is used instead of a solar cell array in the line focus (as shown in Figure 5). However, this should be sufficient to show the basic functionality and to obtain first solar cell efficiencies. A schematic design of the hybrid absorber can be seen in Figure 15. The multi-junction cell (triple-junction cell by the Spanish company Isofoton, up to 37% efficiency, up to 900 suns, 10×10 mm^2) is soldered to a white coated printed circuit board (PCB) consisting of a copper core (DBC) (which also serves as the positive contact), the contact to the negative electrical connection was realized by bonding wires. The PCB is attached to the absorber tube via a copper adapter (compare Section 2.4).

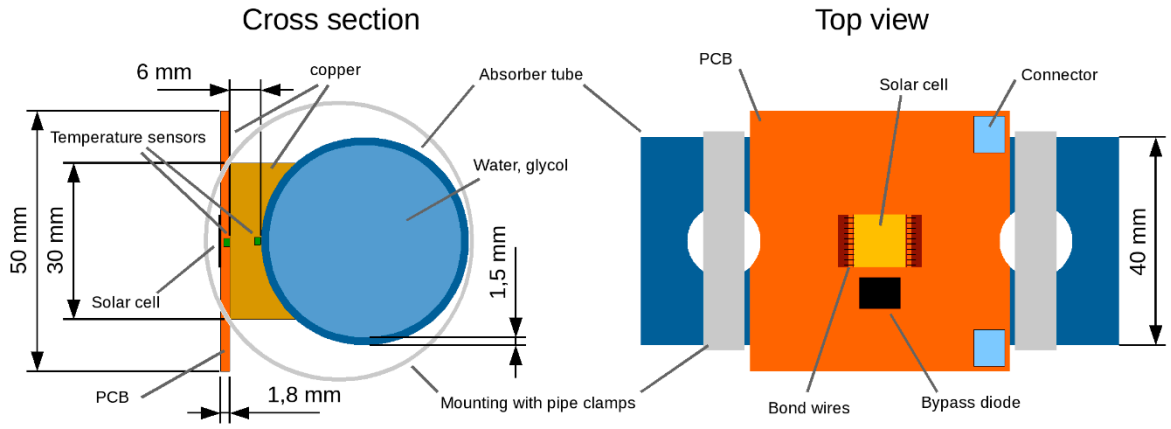

Figure 15. Schematic representation of the hybrid absorber test setup. In order to demonstrate the basic functionality, one multi-junction solar cell is used. Left: Cross section of the absorber tube with good heat conduction (copper adapter) to the solar cell PCB. Right: Front view of the hybrid collector.

For the first feasibility tests, the cylindrical glass envelope, originally surrounding the absorber tube to allow evacuation of the surrounding air and hence increased thermal insulation has been omitted. This results in increased convective cooling of the cell, increased thermal heat losses and no light displacement through the glass.

A water glycol mixture was used as heat transfer fluid (HTF) in the absorber tube. The water flows through a flow meter into a pump to the cooling unit and into the absorber tube before it is fed back into the flow meter. Two temperature sensors measure the water inlet and outlet temperature at the absorber tube. Figure 16 schematically shows the hydraulic system.

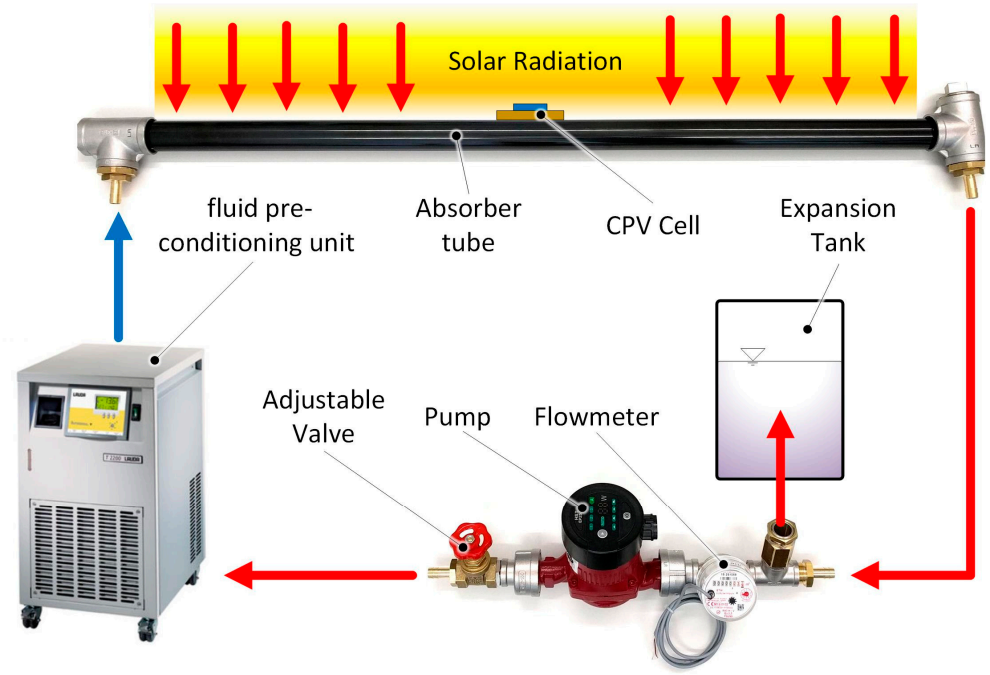

Figure 16. Schematic representation of the test setup's hydraulic system. The temperature sensors are attached to the end caps of the absorber tube.

In the following the different data sources, setups and settings are explained to make the measurements results more comprehensible.

Data sources and settings:

- Irradiance: The global horizontal irradiance (GHI, 10 min average) and air temperature was measured by a nearby (2.5 km) national monitoring station (ZAMG) [37]. In the following measurements, the DNI (direct normal irradiance, which is commonly used in these applications) is calculated from the GHI, assuming that 89% of the GHI corresponds to the DNI (same as in the standardized AM 1.5 spectrum) [31].
- Tracking: The parabolic mirror was manually directed towards the sun. The focus of the collector was chosen so that it was aligned as precisely as possible to the solar cell. The movement of the sun, only allowed measurement periods of several minutes.
- Temperatures: Two calibrated PT100 temperature sensors were used to measure the water/glycol (HTF) temperature at the inlet and outlet of the absorber tube. Additional NTC temperature sensors were used to measure the temperatures at the solar cell and the absorber tube (see Figure 15). All temperature sensors were recorded via a *Rigol M300* digital multimeter. A common domestic hot water flow meter was used to determine the flow of water. A *Lauda T2200* was used as a cooling and water conditioning unit. The thermal power can be calculated from the flow rate of the heat transfer fluid and the temperature difference (4190 J/(kg K) was used as specific heat capacity).

- Electric Power: The solar cell was measured mainly according to the 4-wire method (a small 2-wire section was compensated afterwards). The cell was connected to an electrical load (*RND 320 KEl103*). Current and voltage were each measured with a multimeter (*Rigol DM3058E*). To determine the maximum power point (MPP), the IV-curve of the solar cell was measured automatically using a script running on a "Raspberry Pi" (note that this increases the overall cell temperature since the MPP was not always adjusted).

3.2. Measurements as the Line Focus Passes over the Solar Cell

In this test, the basic functionality of the hybrid absorber was tested, and it was analyzed how the solar cell behaves at different positions of the line focus. The measurements took place on 12 August 2019, in Graz, Austria, under perfect weather conditions (clear sky). The global radiation was 699 W/m^2 and the ambient air temperature was 31 °C. The water glycol mixture used as heat transfer fluid (HTF) in the absorber tube, had a flow rate of 12 L/min. The distance between the absorber tube and the parabolic mirror was adjusted in such a way that the focal point is approximately on the center of the solar cells (adjusted based on optical estimation, compare Section 2.2). The parabolic mirror was aligned, so that the line focus moves over the solar cell due to the movement of the sun. The automatic tracking system of the SMT-8 was switched off during the measurement to eliminate this possible error source and rely solely on the movement of the sun. Figure 17 shows the measured temperature curves and the electrical power output of the solar cell. It can be seen that the cell power increases (line focus moves towards the cell center), reaches a peak at 15:02:30 (line focus exactly on the cell center) and then decreases again (line focus moves away from the cell center). Accordingly, the temperatures at the solar cell also rises or falls. Figure 18 shows the line focus at the maximum power output of the solar cell.

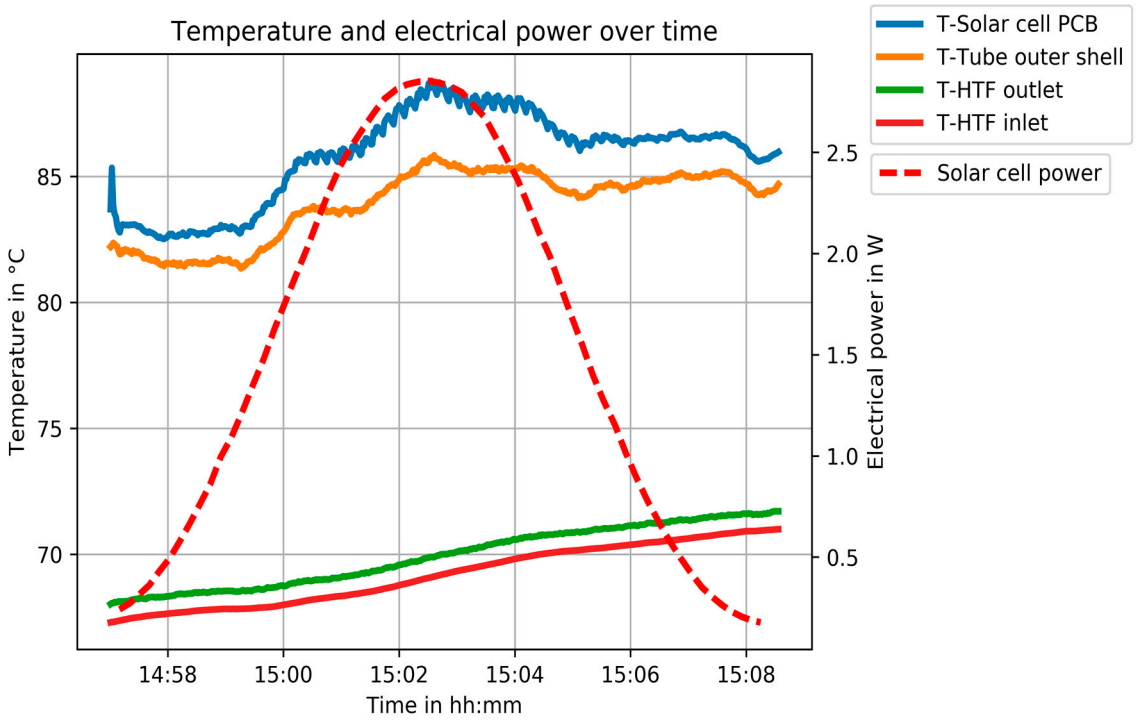

Figure 17. The temperatures (continuous lines) and the power of the solar cell (maximum power point (MPP); dashed line) shown over time. The tracking system is switched off. As the sun moves, the line focus of the concentrated sunlight passes over the solar cell and reaches the cell center at 15:02:30. The sinusoidal course of the power output is due to the movement of the sun, the data were not filtered.

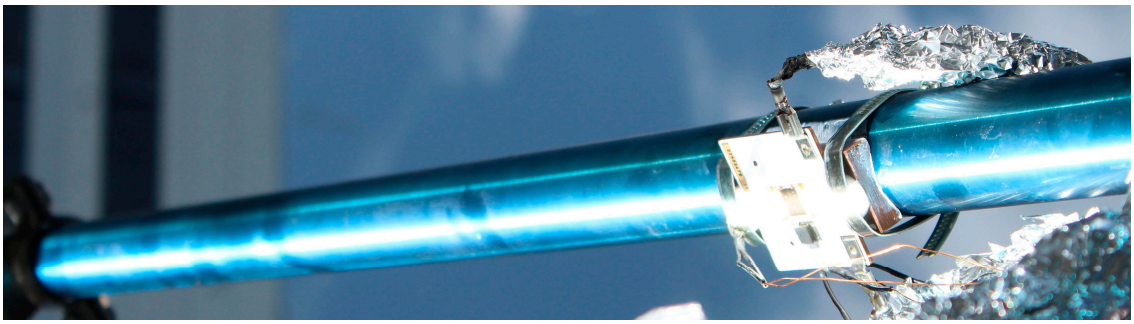

Figure 18. Clearly visible line focus on the absorber tube during the measurements. It can be seen that the line focus is exactly on the solar cell. The challenge for the tracking system is to achieve this permanently.

The maximum electrical power of the 10×10 mm^2 Isofoton solar cell reached 2.85 W. The HTF had 70 °C at that time, while a temperature of 89 °C was measured on the backside of the cell. This results in a temperature difference of approximately 19 K between cell and average HTF. It should be noted that the heating process has not completely settled to a stationary state due to the short duration.

Furthermore, it can be seen that the largest temperature difference occurs between the average HTF temperature (T-HTF outlet) and the absorber tube outer shell (T-Tube outer shell). In comparison, a much smaller difference (3 K vs. 16 K) occurs between the solar cell (T-Solar cell PCB) and the absorber tube outer shell (T-Tube outer shell). Thus, to reduce the overall temperature difference, the heat transfer between the average HTF and the absorber tube outer shell should be improved. This could be done by using tube inlays, fins inside the absorber tube, or higher HTF flow velocities (these investigations will be presented in a separate publication).

In addition, small periodic temperature ripples on the solar cell (T-Solar cell PCB) can be detected. This is due to the IV-curve measurement of the cell. When the cell is operating at the maximum power point (MPP), more power is dissipated electrically and consequently there is less thermal excess and the temperature drops. If, on the other hand, only the open-loop voltage of the cell is measured, almost no power is dissipated electrically and therefore the waste heat is higher and a temperature peak occurs.

The following recorded data was used to determine the efficiency of the solar cell:

$$\eta\text{GHI} = \frac{P\text{out}}{GHI * W * S} = \frac{2.85}{699 * 0.01 * 2.2} = 18.5\% \quad (1)$$

$$\eta\text{DNI} = \frac{P\text{out}}{GHI * F * W * S} = \frac{2.85}{699 * 0.89 * 0.01 * 2.2} = 20.8\% \quad (2)$$

- Global Horizontal Irradiance in W/m^2.
- Direct Normal Irradiance in W/m^2.
- width of the cell in m.
- span width of the parabolic mirror in m.
- Conversion factor between GHI to DNI: 89%.

The electrical efficiency of 20.8% (based on DNI, see Table 5) is relatively low for multi-junction cells but represents a first feasibility study rather than a performance evaluation of a well-tuned and optimized design. The thermal output during this measurement was about 670 W, which is relatively small due to convection losses (~50% efficiency based on DNI) caused by the absence of a vacuum glass envelope. All in all, the operating principle of the hybrid system could be shown successfully.

Table 5. Essential results of the measurement. T-HTF Outlet is the heat transfer fluid outlet temperature and T-Solar Cell PCB is the temperature on the bottom side of the PCB.

Time	T-HTF Outlet	T-Solar Cell PCB	ΔT	$P_{electrical}$	η_{GHI}	η_{DNI}
hh:mm:ss	**°C**	**°C**	**K**	**W**	**%**	**%**
15:02:30	70	89	19	2.85	18.5	20.8

3.3. Effect of the Heat Transfer Fluid Temperature on Cell Efficiency

In this experiment the aim was to improve the efficiency of the solar cell and to apply different heat transfer fluid (HTF) temperatures to analyze the effects on the hybrid absorber. The measurements took place on 12 September 2019 in Graz, Austria under perfect weather conditions (clear sky). The global radiation was 746 W/m^2 and the ambient air temperature was 24 °C. The water glycol mixture used as HTF in the absorber tube had a flow rate of 12 L/min. This time the distance between the absorber tube and the parabolic mirror was adjusted more precisely: Using the short-circuit current of the solar cell, the distance was varied until a maximum current was reached (focal point is on the center of the solar cell).

The parabolic mirror was aligned so that the line focus was directly on the center of the solar cell. Around noon, the movement of the concentrated sunlight across the receiver is the slowest, so that approximately the same conditions could be maintained during the whole measurement. The automatic tracking system was switched off during the measurement.

Figure 19 shows the measured temperature curves and the electrical power output of the solar cell. It can be seen that due to the improved position of the hybrid absorber, the power output of the solar cell is much higher compared to the first measurements in Section 3.2. In addition, a more consistent power output can be seen due to the similar line focus positions on the cell.

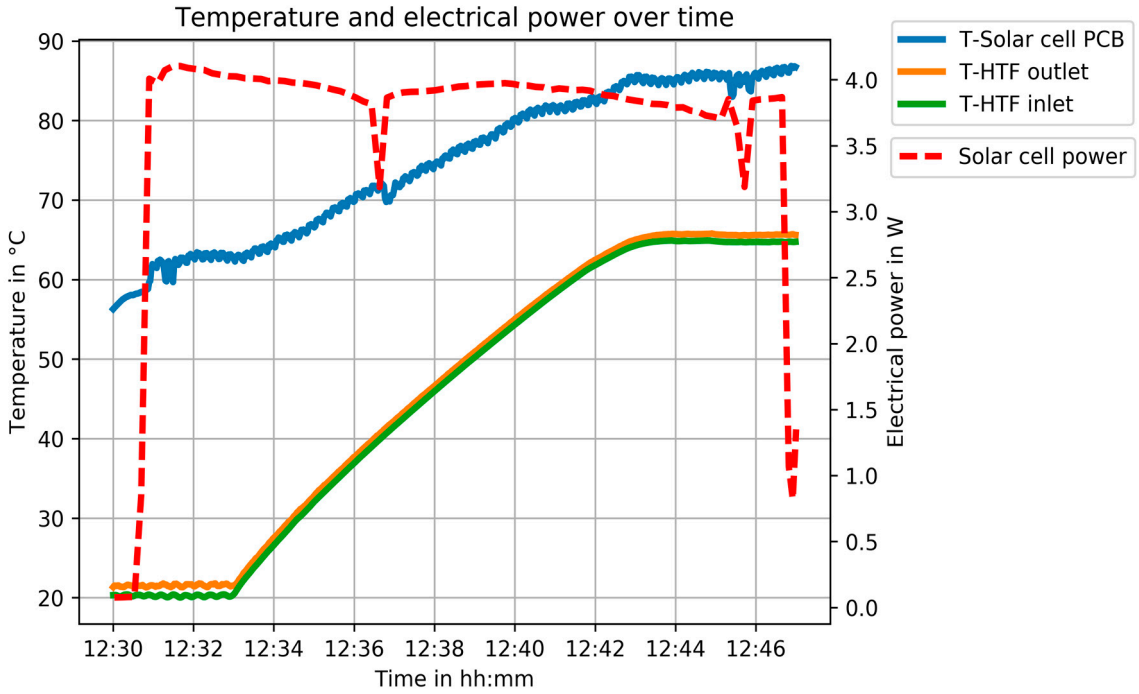

Figure 19. The temperatures (continuous lines) and the power of the solar cell (MPP; dashed line) shown over time. Due to the noon time there is less sun movement. This was used to change the temperature under similar conditions. It can be seen that the temperature difference between cell and heat transfer fluid decreases with increasing water temperature and at the same time the solar cell output decreases. At 12:36:40 and 12:45:40 the tracking system was manually readjusted.

The maximum electrical power of the 10 × 10 mm^2 solar cell reaches 4.1 W (see Figure 20). The measurement started with a HTF temperature of 20 °C, followed by a transition to 65 °C, which was kept constant afterwards. It can be seen that the temperature differences between HTF (T-HTF outlet) and solar cell (T-Solar cell PCB) are larger (in comparison to the last test in Section 3.2), due to the more precise alignment of the line focus and the higher irradiance.

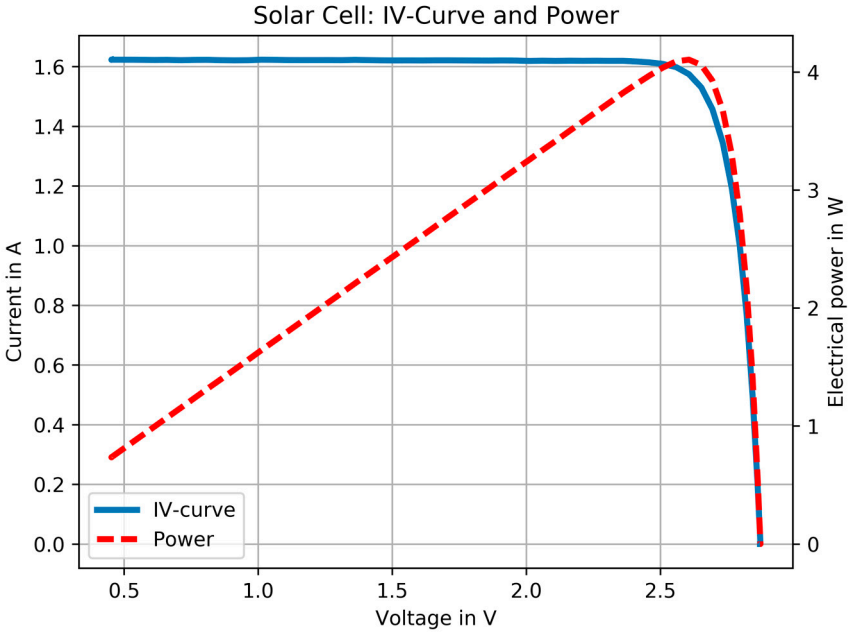

Figure 20. IV-curve and electrical power of the solar cell measured at 12 h:31 min:36 s (focus on the center of the cell). The maximum power point (MPP) of 4.1 W at 2.6 V can be seen.

The efficiency of 28.1% (based on DNI, see Table 6) is much better, primarily due to the more precise positioning of the cell within the focal plane of the parabolic collector and secondly also due to the lower cell temperature. This shows how important the exact positioning of the cell/hybrid absorber is. Nevertheless, there is still potential for further improvements (e.g., optical accuracy, irradiation distribution, heat transfer, and angle of incidence).

Table 6. Essential results of the measurement. Same efficiency calculations as in previous measurement (see Section 3.2).

Time	T-HTF Outlet	T-Solar Cell PCB	ΔT	$P_{electrical}$	η_{GHI}	η_{DNI}
hh:mm:ss	**°C**	**°C**	**K**	**W**	**%**	**%**
12:31:36	21	62	41.0	4.10	25.0	28.1
12:46:34	65.5	86	20.5	3.87	23.6	26.5

From the obtained data the temperature coefficient of the solar cell can be calculated:

$$\alpha = \frac{\eta_{\text{DNI Hot}} - \eta_{\text{DNI Cold}}}{T_{\text{CPV PCB Hot}} - T_{\text{CPV PCB Cold}}} = \frac{26.5\% - 28.1\%}{86\ ^\circ\text{C} - 62\ ^\circ\text{C}} = -0.067\%/K \quad (3)$$

The calculated temperature coefficient of −0.067%/K fits to the coefficients of multi-junction cells (around −0.045%/K), commonly found in datasheets [6].

Furthermore, it can be seen that the temperature difference between cell (T-Solar cell PCB) and HTF (T-HTF outlet) decreases with increasing HTF temperature. From 41 K (at 21 °C HTF temperature) to 20.5 K (at 65.5 °C HTF temperature). This can be explained by the increasing Reynolds number

within the HTF resulting in an improved heat transfer between HTF and absorber tube outer shell. The increase of the Reynolds number results from the viscosity changes of the HTF.

The thermal output during this measurement was ~1100 W at 20 °C HTF temperature (75% efficiency based on DNI) and ~750 W at 65 °C HTF temperature (51% efficiency based on DNI). The large difference in thermal efficiency can be explained through convection losses and shows the importance of a glass envelope and the evacuation of the surrounding air at higher temperatures.

4. Conclusions and Outlook

The tests and measurements within this presented project successfully demonstrated the proof of concept of a solar-thermal "hybrid absorber". The results indicate that is possible to retrofit a convectional parabolic trough collector used in purely thermal systems with multi-junction solar cells to generate electrical and thermal energy at the same time. A solar cell efficiency of 28% (based on DNI) could be successfully achieved without complex secondary optics. It could be shown that the focus on the solar cell must be adjusted very precisely, otherwise, there are significant electrical efficiency losses. Furthermore, the design of an elaborate heat rejection system is key in order to properly address the trade-off between the lowest possible cell operating temperature and the highest possible heat transfer fluid (HTF) temperature. The study showed, that the cell could be successfully operated at temperatures of up to 86 °C, while still offering 26.5% degree of efficiency and allowing HTF temperatures of around 65 °C. A variety of industrial applications requiring heat and electricity in the relevant range were also presented and serve as possible future application for the featured technology.

Based on these first promising results and the successful proof of concept the decision was made to further pursue the hybrid absorber approach. A hybrid absorber containing 2 × 26 10 × 10 mm^2 azure space multi-junction cells (as shown in Figure 21) was designed and is currently undergoing field testing, showing promising first results. Measures to fine-tune the entire system related to optical properties and tracking are planned to further increase the efficiency of the solar cell.

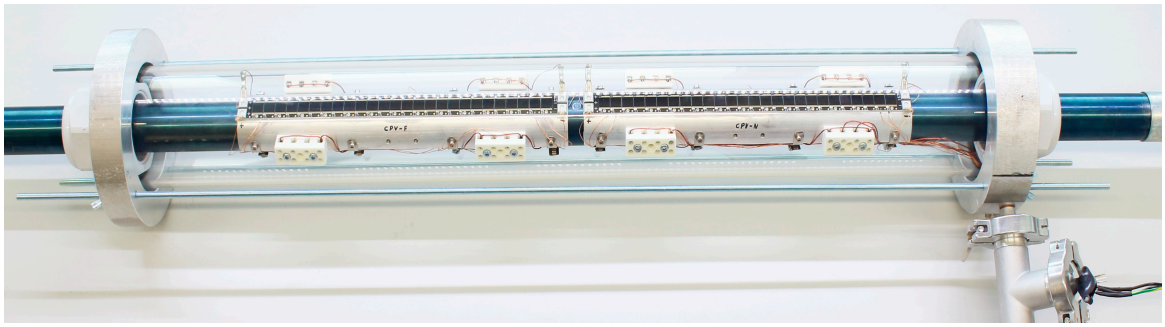

Figure 21. Next-generation CPV-T hybrid absorber designed based on the results of this presented research. This design is currently undergoing field testing.

A significant reduction of the temperature difference between HTF and solar cell is another development target that may be reached using certain tube geometries that alter the flow conditions, as well as thin-walled designs. In the final evaluation of the follow-up project, the overall efficiency ratio—thermal to electrical—will be determined and a Sankey diagram taking into account all losses of the hybrid CPV-T system will be considered. Test results are expected to be published within the near future.

Author Contributions: Conceptualization, R.F., A.B., B.G. and H.W.; Data curation, R.F.; Formal analysis, R.F.; Funding acquisition, A.B. and H.W.; Investigation, R.F., A.B. and B.G.; Methodology, R.F. and B.G.; Project administration, R.F., A.B. and H.W.; Resources, A.B. and H.W.; Software, R.F.; Supervision, A.B. and H.W.; Validation, R.F. and B.G.; Visualization, R.F., A.B. and B.G.; Writing—original draft, R.F., A.B. and B.G.; Writing—review & editing, R.F., A.B., B.G. and H.W. All authors have read and agreed to the published version of the manuscript.

Funding: This research was funded by the Austrian Research Promotion Agency (grant number 865065) with the Energy Research Programs, 4th Call. Open Access Funding by the Graz University of Technology.

Conflicts of Interest: The authors declare no conflict of interest.

References

1. International Energy Agency. Solar PV—Tracking Clean Energy Progress. 14 December 2018. Available online: https://www.iea.org/tcep/power/renewables/solar/ (accessed on 15 February 2019).
2. Trieb, F.; Schillings, C.; O'Sullivan, M.; Pregger, T.; Hoyer-Klick, C. Global potential of concentrating solar power. In Proceedings of the SolarPaces Conference, Berlin, Germany, 15–18 September 2009.
3. Butti, K.; Perlin, J. *A Golden Thread: 2500 Years of Solar Architecture and Technology*; Cheshire Books: Palo Alto, CA, USA, 1980.
4. Ho, C.K.; Sims, C.A.; Christian, J.M. Evaluation of glare at the Ivanpah Solar Electric Generating System. *Energy Procedia* **2015**, *69*, 1296–1305. [CrossRef]
5. Pérez-Higueras, P.; Fernández, E.F. High Concentrator Photovoltaics. In *Fundamentals, Engineering and Power Plants*; Springer: Cham, Switzerland, 2015.
6. Azur Space Solar Power GmbH. Concentrator Triple Junction Solar Cell (Datasheet). 2016. Available online: http://www.azurspace.com/images/products/0004355-00-01_3C44_AzurDesign_10x10.pdf (accessed on 10 October 2020).
7. Wiesenfarth, M.; Philipps, S.P.; Bett, A.W.; Horowitz, K.; Kurtz, S. *Current Status of Concentrator Photovoltaik (CPV) Technology*; U.S. Department of Energy: Washington, DC, USA, 2017.
8. Nreal. Best Research-Cell Efficiency Chart. 2020. Available online: https://www.nrel.gov/pv/assets/pdfs/best-research-cell-efficiencies.20200925.pdf (accessed on 10 October 2020).
9. Fraunhofer. Photovoltaics Report. 2020. Available online: https://www.ise.fraunhofer.de/content/dam/ise/de/documents/publications/studies/Photovoltaics-Report.pdf (accessed on 10 October 2020).
10. Vannoni, C.; Battisti, R.; Drigo, S. Potential for Solar Heat in Industrial Processes. In *IEA SHC Task 33 and SolarPaces Task IV: Solar Heat in Industrial Processes*; CIEMAT: Madrid, Spain, 2008.
11. Palenzuela, P.; Alarcón-Padilla, D.-C.; Zaragoza, G. *Concentrating Solar Power and Desalination Plants—Engineering and Economics of Coupling Multi-Effect Distillation and Solar Plants*; Springer: Cham, Switzerland, 2015.
12. Al-Shammiri, M.; Safar, M. Multi-effect distillation plants: State of the art. *Desalination* **1999**, *126*, 45–59. [CrossRef]
13. Mugnier, D.; Jakob, U. Status of solar cooling in the World: Markets and availableproducts. *WIREs Energy Environ.* **2015**, *4*, 229–234. [CrossRef]
14. Weiss, W.; Spörk-Dür, M. *Solar Heat Worldwide*; Institute for Sustainable Technologies: Gleisdorf, Austria, 2018.
15. Allouhi, A.; Fouih, Y.E.; Kousksou, T.; Jamil, A.; Zeraouli, Y.; Mourad, Y. Energy consumption and efficiency in buildings: Current status and future trends. *J. Clean. Prod.* **2015**, *109*, 118–130. [CrossRef]
16. Thür, A.; Calabrese, T.; Streicher, W. Smart grid and PV driven ground heat pump as thermal battery in small buildings for optimized electricity consumption. *Solar Energy* **2018**, *174*, 273–285. [CrossRef]
17. Selke, T.; Schlager, T.; Rennhofer, M.; Heinz, A.; Brandl, D.; Mach, T. Multifunctional Facade with PV for Solar Autonomous Cooling Applications. In Proceedings of the ISES Solar World Congress 2017 with IEA SHC International Conference on Solar Heating and Cooling for Buildings and Industry, Abu Dhabi, UAE, 29 October–2 November 2018.
18. Euroheat & Power. Ecoheatcool: European Heating and Cooling Market Study. 2006. Available online: https://www.euroheat.org/our-projects/ecoheatcool-european-heating-cooling-market-study/ (accessed on 10 October 2020).
19. Omar, M.; Sharaf, Z. Concentrated photovoltaic thermal (CPVT) solar collectorsystems: Part I—Fundamentals, design considerations and current technologie. *Renew. Sustain. Energy Rev.* **2015**, *50*, 1500–1565.
20. Gibart, C. Study of and tests on a hybrid photovoltaic-thermal collector using concentrated sunlight. *Solar Cells* **1981**, *4*, 71–79. [CrossRef]
21. Buffet, B.P. Hybrid thermal and photovoltaic concentration collector. In Proceedings of the EC Contractors' Meeting, Brussels, Belgium, 16–17 November 1982.

22. Rios, M.; Edenburn, M.W.; Allen, P.A. Cost effectiveness of concentrating photovoltaic-thermal (PVT) systems vs. side-by-side systems for two intermediate applications. In Proceedings of the IEEE 15th Photovoltaic Specialists Conference, Orlando, FL, USA, 11 May 1981.
23. Coventry, J.S. Performance of a concentrating photovoltaic/thermal solar collector. *Solar Energy* **2005**, *78*, 211–222. [CrossRef]
24. Del Col, D.; Bortolato, M.; Padovan, A.; Quaggia, M. Experimental and numerical study of a parabolic trough linear CPVT system. *Energy Procedia* **2014**, *57*, 255–264. [CrossRef]
25. Bellini, E. Concentrating Photovoltaic-Thermal System with 91% Efficiency. Available online: https://www.pv-magazine.com/2020/10/06/concentrating-photovoltaic-thermal-system-with-91-efficiency/ (accessed on 15 October 2020).
26. Riahia, A.; Ben, A.; Fadhel, A.; Guizani, A.; Balghouthi, M. Performance investigation of a concentrating photovoltaic thermal hybrid solar system combined with thermoelectric generators. *Energy Convers. Manag.* **2020**, *205*, 112377. [CrossRef]
27. Yang, F.; Wang, H.; Zhang, X.; Tian, W.; Hua, Y.; Ding, T. Design and experimental study of a cost-effective low concentrating photovoltaic/thermal system. *Solar Energy* **2018**, *160*, 289–296. [CrossRef]
28. George, M.; Pandey, A.K.; Rahim, N.A.; Saidur, R. Recent studies in concentrated photovoltaic system (CPV): A review. In Proceedings of the 5th IET International Conference on Clean Energy and Technology (CEAT2018), Kuala Lumpur, Malaysia, 5–6 September 2018; pp. 1–8.
29. Tao, M. *Terawatt Solar Photovoltaics—Roadblocks and Opportunities*; Springer: London, UK, 2014; pp. 11–20.
30. IXYS Korea Ltd. IXOLAR(TM) High Efficiency SolarBIT (Datasheet). IXYS Corporation. 2011. Available online: https://ixapps.ixys.com/DataSheet/KXOB22-04X3-DATA-SHEET-20110808.pdf (accessed on 10 October 2020).
31. The National Renewable Energy Laboratory (NREL). Reference Air Mass 1.5 Spectra. Alliance for Sustainable Energy LLC. Available online: https://www.nrel.gov/grid/solar-resource/spectra-am1.5.html (accessed on 10 October 2020).
32. Azur Space Solar Power GmbH. *Products CPV—PV Solar Cells*; AZUR SPACE Solar Power GmbH: Heilbronn, Germany. Available online: http://www.azurspace.com/index.php/en/products/products-cpv/cpv-solar-cells (accessed on 10 October 2020).
33. Helmers, H.; Schachtner, M.; Bett, A.W. Investigations on the influence of temperature and concentration on solar cell performances. In Proceedings of the 9th International Conference on Concentrator Photovoltaic Systems (CPV 2013), Miyazaki, Japan, 15–17 April 2013; Available online: http://publica.fraunhofer.de/documents/N-279987.html (accessed on 20 October 2020).
34. Yoon, S.; Garboushian, V. Reduced temperature dependence of high-concentration photovoltaic solar cell open-circuit voltage (Voc) at high concentration levels. In Proceedings of the 1994 IEEE 1st World Conference on Photovoltaic Energy Conversion—WCPEC (A Joint Conference of PVSC, PVSEC and PSEC), Waikoloa, HI, USA, 5–9 December 1994.
35. Kost, C.; Mayer, J.N.; Thomsen, J.; Hartmann, N.; Senkpiel, C.; Philipps, S.; Nols, S.; Lude, S.; Saad, N.; Schlegl, T. *Levelized Cost of Electricity—Renewable Energy Technologies*; Fraunhofer Institute for Solar Energy Systems (ISE): Freiburg, Germany, 2013.
36. Cooper, T.; Ambrosetti, G.; Malnati, F.; Pedretti, A. Experimental demonstration of high-concentration photovoltaics on a parabolic trough using tracking secondary optics. *Prog. Photovolotaics Res. Appl.* **2016**, *24*, 1410–1426. [CrossRef]
37. Zentralanstalt für Meteorologie und Geodynamik (ZAMG). Meteorological Network. Zentralanstalt für Meteorologie und Geodynamik, Hohe Warte 3, 1190 Vienna. Available online: https://www.zamg.ac.at/cms/en/climate/meteorological-network (accessed on 10 October 2020).